Journal of Arid Environments 122 (2015) 1–15

Contents lists available at ScienceDirect

Journal of Arid Environments

journal homepage: www.elsevier.com/locate/jaridenv

Mountain-river runoff components and their role in the seasonal development of desert-oases in northwest China

Mir A. Matin [a], Charles P.-A. Bourque [a, b, *]

[a] Faculty of Forestry and Environmental Management, University of New Brunswick, 28 Dineen Drive, PO Box 4400, Fredericton, New Brunswick, E3B 5A3, Canada

[b] The School of Soil and Water Conservation, Beijing Forestry University, 35 East Qinghua Road, Haidan District, Beijing, 100083, PR China

ARTICLE INFO

Article history:
Received 30 June 2014
Received in revised form
28 April 2015
Accepted 22 May 2015
Available online 15 June 2015

Keywords:
Hydrological cycle
Hydrometric measurements
Vegetation-runoff relationship
Remote sensing
Water-balance calculations

ABSTRACT

The paper examines the role of mountain runoff in the seasonal growth of oasis vegetation in the hyper-arid region of northwest China. Central to this examination is the development of a simple hydrologic model that relates hydrologic inflows and outflows estimated from remote sensing data (e.g., evapotranspiration, precipitation, snow accumulation, and snowmelt) to the calculation of runoff over a ten-year period (2000–2009). Modeled runoff is shown to reproduce the seasonal trends in hydrometric data fairly well, yielding R^2's of 0.75 and 0.66 for stations in the upper reaches of the Shiyang and Hei River systems. Greater than 90% of the runoff from the Qilian Mountains to the oases occurs during the May–September period. Considerable discrepancy between modeled and observed runoff exists in the lower reaches of the rivers, where significant amounts of river water (>45%) are routinely extracted for cropland irrigation. Along the river systems, where water extraction and inflow of glacial meltwater are minor, model calculations replicate observed water yields much more closely. Analysis of seasonal trends in the contribution of snowmelt and rainfall to the return flow, reveals snowmelt as having the greatest influence in initiating the oasis growing period during the March-to-May period of each year.

1. Introduction

Permanence of vegetation cover at the base of mountain ranges in northwest (NW) China is fundamental to the long term ecological integrity of lowland oases (Ji et al., 2006). Desert-oases in the region account for little more than 5% of the total landbase (Han and Meng, 1999; Li et al., 2006), yet support about 95% of the region's growing population (Chu et al., 2005). In the shadow of the Qinghai-Tibetan Plateau, NW China is one of the driest places on earth (Huo et al., 2007). The amount of convective precipitation induced locally (at the scale of individual oases) is normally insufficient to satisfy the demand for water by existing lowland vegetation. Fate of this vegetation depends to a large measure on the availability of substantial amounts of precipitation-water generated in the mountains as a result of orographic processes (Bourque and Hassan, 2009).

Water recycles in these hydrologically-closed (endorheic) basins through three main mechanisms, namely through: (i) the loss of oasis surface water to the atmosphere by evapotranspiration (ET) and horizontal wind advection; (ii) the production of in-mountain precipitation by orographic lifting of moistened desert air and condensation of water vapor; and (iii) the return of liquid water to the base of the mountains and oases by downslope, surface and shallow-subsurface flow (Bourque and Hassan, 2009; Bourque and Matin, 2012). In general, water not used by the lowland vegetation or by humans flows to terminate in the deserts due to excessive evaporation (Li et al., 2013).

Associated river basins are economically very important (Chen et al., 2003), but at the same time, extremely sensitive to hydro-meteorological and climate variability (Meybeck, 2003). Monitoring and forecasting of water yield and generation of river runoff is crucial to the sustainable management of these basins.

Conceptual hydrological models use simple mathematical equations to describe basic hydrological processes of river basins (Aghakouchak and Habib, 2010) and are based on a schematic understanding of hydrological features (Pechlivanidis et al., 2011). By using simpler equations, conceptual models overcome some of the limitations in physically-based models (Elshorbagy et al., 2010).

* Corresponding author. Faculty of Forestry and Environmental Management, University of New Brunswick, 28 Dineen Drive, PO Box 4400, Fredericton, New Brunswick, E3B 5A3, Canada.

E-mail addresses: m.matin@unb.ca (M.A. Matin), cbourque@unb.ca (C.P.-A. Bourque).

http://dx.doi.org/10.1016/j.jaridenv.2015.05.011
0140-1963/

Their simplicity, however, has resulted in some opposition from hydrologists because of the lack of causal description of physical relationships (Elshorbagy et al., 2009). In spite of this opposition, when implemented with prudence and an excellent understanding of the interactions among the different variables, conceptual models are convenient tools in modeling hydrological systems. Popular conceptual models varies in terms of spatial representation, number of calibration parameters, and level of process description. In simplifying calculations, semi-distributed models, such as TOPMODEL (Beven and Kirkby, 1979), HBV (Lindstrom et al., 1997), and SWAT (Arnold et al., 2012), partition river basins into homogenous response units (sub-catchments) according to the region's topography, landuse, and other land-surface features. TOPMODEL and SWAT require the calibration of 11 parameters and HBV, the calibration of 17 parameters in their basic use. The distributed model, variable infiltration capacity model (VIC), partitions the watershed into equal grid areas and requires the calibration of 17 parameters.

Few attempts have been made to implement hydrological models in simulating river runoff in NW China. Chen et al. (2003) implemented a distributed model for a mountainous region of the Hei River basin. In their work, the study area was sub-divided into 103 sub-basins; each sub-basin providing a new background for the calculation of water balances at the sub-basin scale. Excess water in each sub-basin (i.e., water beyond the water-holding capacity of sub-basins) was treated as runoff and was passed on to a neighboring sub-basin in a downstream direction. The model required that 27 parameters be calibrated. Kang et al. (1999) implemented the HBV model with some modification. Using precipitation and temperature as basic input, the model generated monthly ET and surface runoff. Vertical modification in precipitation and temperature fields was calculated from altitudinal gradients and atmospheric lapse rates estimated from meteorological data acquired from the Zhangye (reference station) and surrounding climate stations. Zhao and Zhang (2005) employed the VIC-3L model for the headwaters of the Hei River basin. VIC-3L is a grid-based model (Liang et al., 1996) that generates surface runoff depth within individual grid cells. Surplus water is routed in the model according to a unit-hydrograph method (Nijssen et al., 1997); a unit hydrograph is the direct runoff resulting from one unit of effective rainfall (Rakhecha and Vijay, 2009). Input data to the model were interpolated from daily precipitation and temperature data observed at several climate stations. Jia et al. (2009) implemented a distributed water- and energy-balance model to investigate the hydrological cycle in the upper and middle reaches of the Hei River basin. Model simulations were performed with daily precipitation and temperature input data at 1-km grid resolution generated with Thiessen polygons and adjusted locally according to elevation.

Common to all of these applications is the engagement of some form of numerical interpolation in generating the required input data. As the models are complex, model calibration (given the appropriate information) frequently relies on adjusting a large number of model parameters, usually by trial and error. In general, as the number of model parameters increases, the statistical stability of model predictions deteriorates (Xing et al., 2008). Also, the spatial unit of calculation is often large, e.g., at the sub-basin scale or at coarse grid resolutions ($\geq$1-km resolution). Depending on the sensitivity of parameters, calibration error in these models can often lead to incorrect results; this is particularly the case in areas with highly variable landcover and topography, such as in NW China. Lack of computing resources may also limit the application of these complex models, especially when spatial resolutions are refined or the models are applied to large computational domains (Kishtawal et al., 2003).

Quality of the output from hydrological models is always determined by the quality of input data used in model calibration, initialization, and simulation. In sparsely-gaged river basins, application of distributed models may suffer some uncertainty, due to error introduced in the input data as a result of spatial interpolation. In regions, where landcover and topographic variation is high, calibrated remote sensing (RS)-data can help improve model-output quality (Schultz, 1993). Various RS-sensors deployed over the last few decades have proven effective either at directly estimating specific hydrologic variables or by capturing land surface and atmospheric properties that can be subsequently used to estimate components of the water cycle (Pietroniro and Leconte, 2005; Schmugge et al., 2002). At present, means to determine river runoff directly from RS-data are lacking. However, earlier studies have shown that the use of RS-data as input in distributed hydrological models can enhance our modeling capabilities of surface runoff (Immerzeel et al., 2008; Liu et al., 2012; Qin et al., 2008; Schultz, 1996; Shelp et al., 2011).

In this study, we develop and implement a monthly distributed hydrological model to estimate surface runoff and river-water yields at moderate spatial resolution (250-m resolution) for two data-sparse, endorheic river basins in NW China over a 10-year period (2000–2009). Considering that most of the liquid water generated in these river basins contributes to surface and sub-surface flow with much less to recharging groundwater, we assume that a simple water-balance model, with fewer parameters than most existing hydrological models (two, overall), is sufficiently robust to produce acceptable evaluations of river runoff, when high-quality input data (i.e., rasterized hydrological components generated from RS-data) are used in model simulation.

2. Study area

The study area consists of the Shiyang and Hei River basins in westcentral Gansu, NW China (Fig. 1). The Shiyang River basin is an endorheic river basin (Li et al., 2013) located in the eastern Hexi Corridor. The Shiyang River network originates from the Qilian Mountains and flows about 300 km northeastward (Gao et al., 2006) before terminating in the Minqin-lake district (Li et al., 2007). The total basin area is roughly 49,500 km^2. Elevation in the Shiyang River basin varies from 1284–5161 m above mean sea level (AMSL), with a mean elevation of 1871 m AMSL. The Shiyang River network has eight main branches, including the Xida, Donga, Xiying, Jinta, Zamusi, Huangyang, Gulang, and Dajing Rivers (Li et al., 2013; Wonderen et al., 2010).

The Hei River network also originates in the Qilian Mountains, northwest of the main source of the Shiyang River, and flows northwestward through the oases and terminates in the desert lakes (Akiyama et al., 2007). The Hei River basin, with a land surface area of approximately 128,000 km^2, is the second largest endorheic river basin in NW China (Gu et al., 2008). The Hei River basin includes the Zhangye sub-basin, with a total land area of about 31,100 km^2. Elevation in the Zhangye sub-basin varies from 1287–5045 m AMSL, with a mean elevation of 2679 m AMSL (Fig. 1).

The study area overlaps four distinct ecoregions (Olson et al., 2001). The northern part, noted for its arid to semi-arid conditions, includes a portion of the Badain Jaran and Tengger deserts and oases in the southwestern portions of the Alashan Plateau. The Liangzhou Oasis, to the south, and the Minqin Oasis, to the north, are two important oases in the Shiyang River basin (Li et al., 2007), whereas the Zhangye Oasis is the main oasis in the Zhangye sub-basin. Spring wheat is the main food crop grown in these oases, which is usually supported by irrigation (Zhao et al., 2005). In the deserts, salt-tolerant, xerophytic shrub species, i.e., saxaul

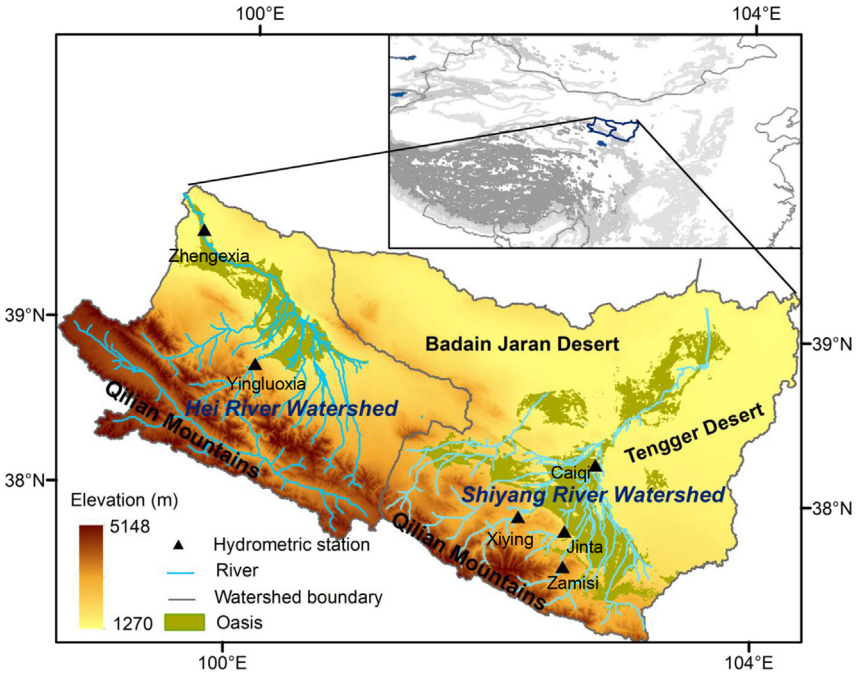

Fig. 1. The Shiyang and Hei River basins. The inset shows the location of the study area along the northeastern flank of the Qinghai-Tibetan Plateau. Gray areas in the inset represent mountain ranges and plateau. Location of hydrometeric stations relevant to the study are also indicated.

(*Haloxylon ammodendron*) and *Reaumuria soongolica* (Carpenter, 2001a) are commonly found. The north-facing slopes of the Qilian Mountains (Fig. 1) support alpine meadow at elevations ≤3300 m AMSL and deciduous shrubland at elevations >3300 m AMSL. Isolated patches of conifer forests (mostly consisting of Qinghai spruce; *Picea crassifolia*) in the Qilian Mountains are classified as a separate ecoregion (Carpenter, 2001b). Various components of the natural landscape of the study area includes mountains, oases, and deserts, all of which interact with one another (Ma and Veroustraete, 2006).

The study area includes five morphologic units, including mountainous morphologic regions, foothill country, alluvial fans, plain, and terminal lakes (Gao et al., 2006). Umbric soils dominate in the oases of both river basins, i.e., Umbric Leptosols in the Shiyang and Umbric Leptosols and Umbric Gleysols in the Hei River basins, whereas in the mountainous region soil types generally vary as a function of elevation. The dominant soil groups in the mountains are Cambisols, Luvisols, Gleysols, and Pedozols (Nachtergaele et al., 2012). The oases are mostly flat with a mean slope <5°, whereas mountainous regions are highly undulated; roughly 40% of the region has slopes >15°.

There is insufficient precipitation to support agriculture in the oases; Bourque and Hassan (2009) have determined precipitation rates of 120–170 mm yr^{-1} in the oases, based on 30 years of data collected from 1976 to 2005. The oases are largely maintained by the surface runoff generated in the Qilian Mountains, as snowmelt and in-mountain-generated rainfall make their way to the Shiyang and Hei River systems (Jin et al., 2010; Wang et al., 2009a). Glacial meltwater on average contributes to about 3.8 and 8.3% of total runoff in the Shiyang and Hei Rivers, respectively (Wang et al., 2009a).

Meltwater increases river flows principally in late spring-to-mid-summer due to the melting of the previous snow-season's snow cover and warming of the mountain glaciers (Ji et al., 2006). The primary source of water to the rivers during the summer is orographic precipitation (Roe, 2005) induced by the Qilian Mountains (Zhu et al., 2004). Long term average data (1950–2000) show that precipitation and potential ET (based on calculations with the Penman-Monteith equation; Monteith, 1965; Penman, 1948) in the deserts are approximately 80–150 mm yr^{-1} and 2300–2600 mm yr^{-1}, respectively. Corresponding figures for the mountainous regions are 300–600 mm yr^{-1} for precipitation and about 700 mm yr^{-1} for potential ET (Akiyama et al., 2007; Chen et al., 2005; Gates et al., 2008; Huo et al., 2008; Kang et al., 2009; Ma et al., 2013; Tong et al., 2007; Wang and Cheng, 1999; Wang and Zhao, 2011; Zang et al., 2012). Most of the precipitation occurs during the June-through-August period of the year. Mean annual runoff in the Shiyang River is about 15.75×10^8 m^3 yr^{-1}, whereas in the Hei River it is about 37.7×10^8 m^3 yr^{-1} (Kang et al., 2009).

Vegetation in the oases and lower mountains plays an important role in maintaining the hydrological cycle. The water vapor generated by ET is lifted by orographic processes and is the source for the formation of precipitation in the mountains. Interruption of the region's vegetative cover could conceivably lead to a disruption in the eco-hydrological balance in the recycling of water (Bourque and Hassan, 2009), which could potentially reduce the downward flow of surface and shallow-subsurface water that must be supplemented with the unsustainable extraction of groundwater. Dependence of the local water cycle on lowland oasis vegetation is supported by many other studies, including those of Huo et al. (2008), Jia et al. (2010), Kang et al. (1999), Li et al. (2008), and Ma et al. (2013).

3. Model description

In this study, we develop a distributed-hydrological model based on an aggregated response unit (ASA) represented by individual raster-grid cells (Kite and Pietroniro, 1996) at 250-m resolution. A 90-m digital elevation model (DEM) is used to characterize basin morphology, including stream networks. Model inputs, including ET, precipitation, snow accumulation, and snowmelt (also at 250-m resolution; Matin and Bourque, 2013a, 2013b), are generated in part from RS-products and validated against data

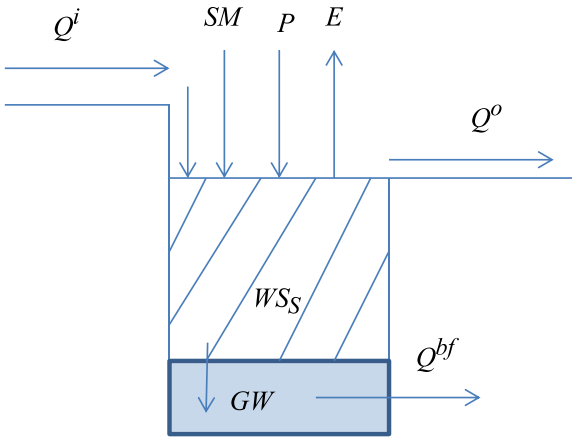

Fig. 2. Schematic of "bucket-model" concept applied in water-balance calculations at each grid cell.

collected at local climate stations (Matin and Bourque, 2013b). The model, based on a "bucket-model" concept, has three main components (Fig 2): i.e., (i) a vertical water-balance calculation executed at individual grid cells; (ii) a soil water-storage component; and (iii) horizontal flow of excess water, including the amounts associated with surface runoff and baseflow.

In the "bucket-model", the soil complex is viewed as the bucket and soil water is balanced through water gains and losses (Huang et al., 1996; Kobayashi et al., 2001; Manabe, 1969; Romano et al., 2011). Change in storage of soil water (in mm) is assessed according to:

$$WS_k = WS_{k-1} + P_k + SM_k - AET_k - GW_k, \tag{1}$$

where WS_k is the soil-water storage during month "k" (k = 1,…,12, from January to December), WS_{k-1} is the soil-water storage during the previous month (k−1), and P_k, SM_k, AET_k, and GW_k are the monthly gains and losses of water associated with rainfall, snowmelt, actual ET (AET), and groundwater recharge (GW) during month k (schematized in Fig. 2); all amounts are in mm.

Saturation-excess storage is calculated as the surplus from accumulated inward bound surface water and the water balance in individual grid cells, i.e.,

$$Q_k^o = \begin{cases} 0.0; & \text{if } Q_k^i + WS_k \le WS_s \\ (Q_k^i + WS_k - WS_s); & \text{if } Q_k^i + WS_k > WS_s \end{cases}, \tag{2}$$

and

$$WS_k = \begin{cases} WS_s; & \text{if } Q_k^i + WS_k > WS_s \\ (Q_k^i + WS_k); & \text{if } Q_k^i + WS_k \le WS_s \end{cases}, \tag{3}$$

where Q_k^i is the sum of all water routed to an individual cell from neighboring cells (this is further addressed in Section 3.5), Q_k^o is the amount of water running out from a particular grid cell to its neighbor downstream, and WS_s is the saturated water-holding capacity of the soil in individual cells (also in mm).

The computational framework of the model is illustrated in Fig. 3. Calculations are carried over a monthly timestep. Steady-state conditions are assumed to hold for all water-balance calculations at the individual cell level. Estimated travel time from upstream to downstream locations is less than one month, based on average flow velocities of 0.4 and 0.05 m s^{-1} in the upper and lower reaches of the watershed (Wu et al., 2004).

3.1. Soil-water storage

In saturated conditions, any water available in the soils beyond field capacity (FC) drains downward as gravitational water (Forth, 1990). Soil water content at FC (i.e., WS_{FC}) is measured at 33 kPa, whereas the permenant wilting point (i.e., the level of non-saturation, below which plants can no longer extract water from the soil; Forth, 1990) is measured at 1500 kPa (Saxton and Rawls, 2006). Saxton and Rawls (2006) derived a set of formulae, based on inputs of % sand, clay, and organic matter to calculate soil water at different soil-water potentials, i.e.,

$$WS_{FC} = WS_{33} + \left[1.283(WS_{33})^2 - 0.374(WS_{33}) - 0.015\right], \tag{4a}$$

$$WS_{33} = -0.251S + 0.195C + 0.011OM + 0.006(S \times OM) - 0.027(C \times OM) + 0.452(S \times C) + 0.299, \tag{4b}$$

$$WS_{S-FC} = WS_{S-33} + (0.636WS_{S-33} - 0.107), \tag{4c}$$

$$WS_{S-33} = 0.278S + 0.034C + 0.022OM - 0.018(S \times OM) - 0.027(C \times OM) - 0.584(S \times C) + 0.078, \tag{4d}$$

and

$$WS_S = WS_{FC} + WS_{S-FC} - 0.097S + 0.043, \tag{4e}$$

where WS_{FC} is the soil water storage at FC of an undisturbed soil complex of normal density, WS_{33} is the FC of the soil in the initial predictive equation that is further adjusted for lack of fit with Eq. (4a), and S, C and OM are the % sand, clay, and organic content of the soil. Similarly, WS_{s-33} is the differences in soil water content between saturation and FC in the first predictive equation that is further adjusted for error in Eq. (4c), and WS_s is the saturated water-holding capacity in an undisturbed soil. Adjustment of the initial predictive equations were done by analyzing an extensive dataset of soil-water characteristics from the USDA/NRCS National Soil Characterization Database. Water volume is derived as a % of a reference soil depth of 1000 mm (Nachtergaele et al., 2012).

Soil parameters for NW China are based on GIS data from the harmonized world soil database (Nachtergaele et al., 2012). The database incorporates the digital soil map of China (1:1,000,000) with organization of the country's soils into 12 orders, 61 great groups and subgroups, and 909 families. Distributed field capacities and saturated water-holding capacities processed for the study area are displayed in Fig. 4.

The model (Fig. 2) computes water available from soil storage on a per cell basis by assuming average soil characteristics and fixed values for soil-water-storage capacities independent of soil depth. As both storage and transmission properties of soils vary with depth, there is clearly opportunity to improve model results when updated values become available. Initial volumes of available soil water are specified at the start of each water-balance calculation.

3.2. Precipitation and snowmelt

Precipitation in the Qilian Mountains has clear seasonal characteristics (Bourque and Matin, 2012; Matin and Bourque, 2013b). During cold weather from September–May, in-mountain precipitation falls mainly as snow and during warm weather in June–August, it falls as rain (Bourque and Matin, 2012). Precipitation

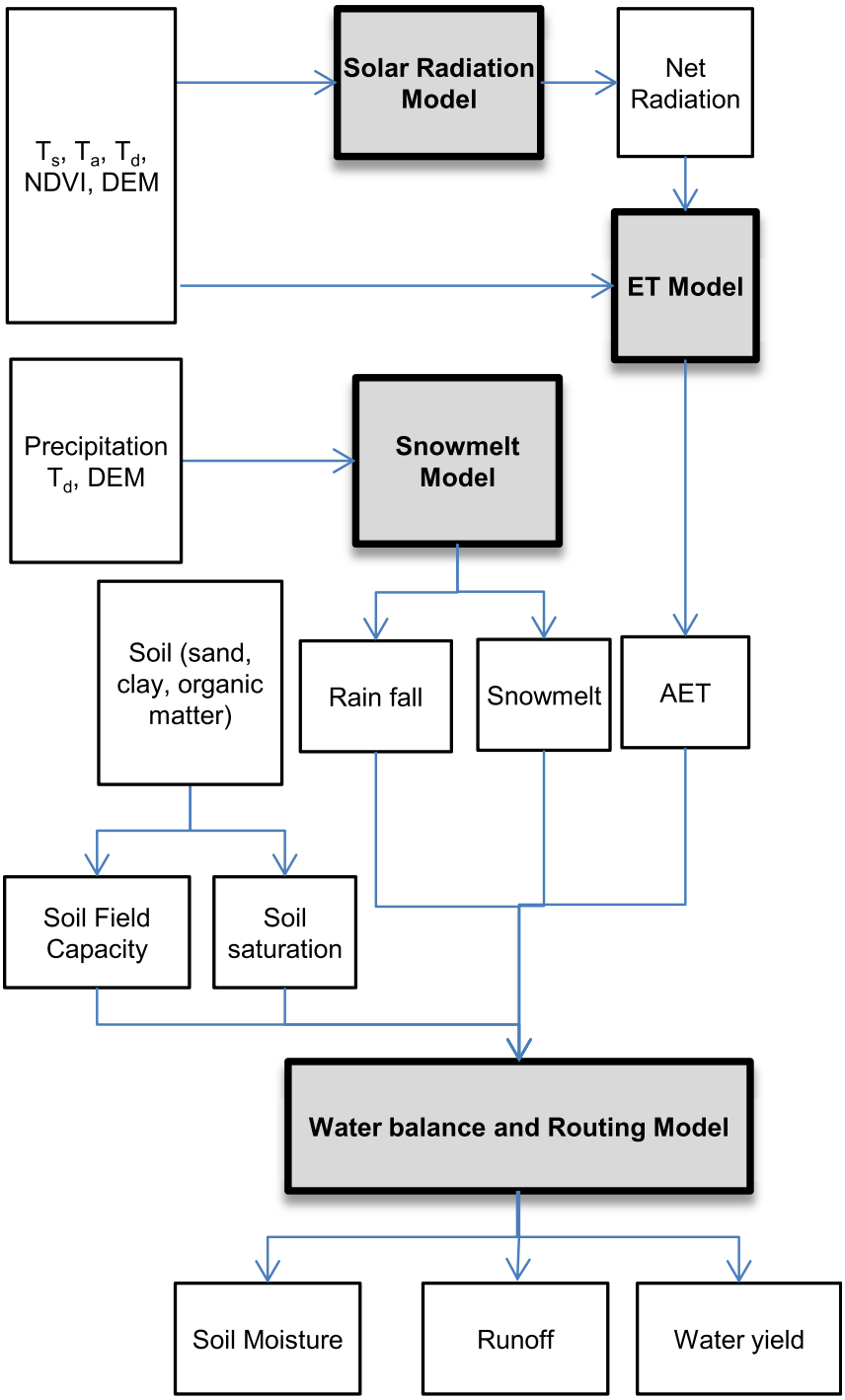

Fig. 3. Workflow regarding individual water-balance calculations and associated inputs and outputs.

ceases to form during the December–February period of each year, including in the mountains, as the air during this time holds very small amounts of water vapor due to plant dormancy and low ET (Bourque and Matin, 2012). Absence of precipitation gages and snow-water monitoring stations in the mountains makes it particularly difficult to get accurate estimates of snow and rainfall volumes for the region. To conduct water-balance calculations and quantify river runoff, we depend on AET (developed by Matin and Bourque, 2013a), precipitation, and snowmelt surfaces developed largely from RS-data and a snow-accumulation and snowmelt model ("snowmelt model", hereafter) formulated in a earlier study (Matin and Bourque, 2013b).

Spatial enhancement of precipitation input was achieved by relating Tropical Rainfall Measuring Mission (TRMM)-precipitation data to Moderate Resolution Imaging Spectroradiometer (MODIS)-based total precipitable water (TPW), relative humidity (RH) calculated from MODIS-based near-surface air and dew-point temperatures (T and T_d), trigonometric functions of time, and DEM-height data (H; Table 1). Spatially-enhanced precipitation images were subsequently adjusted with geographically-weighted regression and observed precipitation from several climate stations within the study area. Adjusted precipitation correlated positively

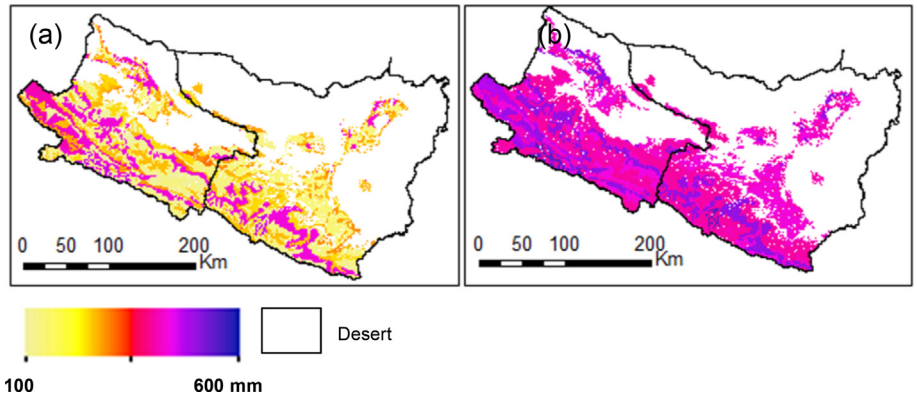

Fig. 4. Soil field capacity (in mm; a) and saturated moisture (mm; b) derived for the study area.

with elevation, including in the lower- to high-mountain portion of the Qilian Mountains (i.e., $R^2 = 0.87$, for precipitation below 3900 m AMSL).

In general, precipitation on the windward-side of major mountain ranges, including the Qilian Mountains, increases with elevation to a certain elevation, beyond which precipitation decreases as the air continues to rise (Bagchi, 1982; Yang et al., 1991), because of diminished moisture (Miller, 1961). Wang and Zhao (2013) found precipitation in the Hei River basin increases up to an elevation of about 3800 m AMSL before decreasing with further lifting of the air. Based on observations in an area next to the Qiyi Glacier (western section of the Qilian Mountains; Wang et al., 2010), Wang et al. (2009b) found the zone of greatest precipitation to occur between 4500–4700 m AMSL. Zone of greatest

Table 1
Input variables and their image-data sources pertinent to the generation of AET, precipitation, and snowmelt surfaces for water-balance calculations, including their spatiotemporal resolutions (columns 3 and 4) before and after spatial enhancement. Bracketed values are not given in cases where there is no spatial enhancement or temporal aggregation applied (modified from Matin and Bourque, 2013b).

Variables	Product generation or source	Spatial	Temporal[a]
		Original (after processing) (m)	Original (after processing)
Normalized difference vegetation index (NDVI)[a] Enhanced vegetation index (EVI)[a,b]	MODIS vegetation indices [MOD13Q1 (Huete et al., 2002; Huete et al., 1997; Wan et al., 2004)].	250	16 day (1 month)
Land surface temperature (T_s)[a,b]	MODIS land surface temperature (MOD11A2; Wan et al., 2004); monthly averages were produced by weighted averaging of 8-day composites. The original 1000-m resolution was enhanced to 250 m using MODIS EVI (at 250-m resolution) as primary predictor; processing steps are outlined in Section 3.2.1 (steps 1–6; in Matin and Bourque, 2013b).	1000 (250)	8 day (1 month)
Land surface emissivity (ε_s)[a]	MODIS land surface emissivity was derived by averaging MODIS-bands 31 and 32 emissivity (Petitcolin and Vermote, 2002)	1000	8 day (1 month)
Land surface albedo (A_s)[a]	MODIS products combined with BRDF-albedo products (MCD43B3; Davidson and Wang, 2005)	1000	16 (1 month)
Air temperature (T)[a,b] Dew-point temperature (T_d)[a,b]	MODIS atmospheric profile data (MOD07; Seeman et al., 2006); near surface temperature are extracted at the pressure level closest to the ground-surface described by the region's digital elevation model (DEM). Daily data were averaged to generate monthly averages. Original T-images were digitally enhanced to 250 m by relating their values to enhanced T_s; 5000-m resolution images of MODIS-T_d were enhanced to 250 m by relating to MODIS EVI (250 m) and enhanced T_s. Both T and T_d were calibrated and validated against independent climate-station data (Matin and Bourque, 2013b, Fig. 3).	5000 (250)	1 day (1 month)
Relative humidity (RH)[b]	Relative humidity (250-m resolution) was calculated as the ratio of actual vapor pressure to saturated vapor pressure calculated from monthly T and T_d (Bourque and Hassan, 2009), both at 250-m resolution.	250	1 month
Total precipitable water (TPW)[b]	MODIS near infrared daily total precipitable water product (MOD05; Gao and Kaufman, 2003; Kaufman and Gao, 1992); monthly values were generated by averaging daily daytime values.	1000	1 day (1 month)
Elevation (H)[a,b]	Shuttle Radar Topographic Mission (SRTM) DEM; gap-filled version (v. 4) obtained from the Consortium of Spatial Data and Information (CGIAR-CSI, 2008; Reuter et al., 2007).	90	n/a[c]
Net radiation and soil heat flux (i.e., R_n-G)[a]	Calculated from estimated incoming solar radiation obtained with the Solar Analyst tool in ArcGIS and SRTM-DEM height data, and RS-based A_s, T, and T_s images in estimating outgoing and incoming reflected shortwave and longwave radiation surfaces for R_n and a NDVI-based correction of incident solar radiation for G (Matin and Bourque, 2013a).	250	n/a

[a] Variables used in the calculation of AET.
[b] Precipitation-related variables used in the digital enhancement of TRMM-data.
[c] n/a = not applicable.

precipitation is documented to vary according to location in the Qilian Mountains and time of year (Wang and Zhao, 2013) and its position is largely correlated to the amount of water vapor in the air and timing of oasis-vegetation development and recession (Bourque and Hassan, 2009; Bourque and Matin, 2012). As a result, the absence of high-elevation climate stations in the Qilian Mountains tends to constrain our understanding of orographic phenomenon in the upper Qilian Mountains.

Development of input precipitation surfaces, as described in Matin and Bourque (2013b), may have introduced a level of overestimation in the upper mountains. To correct this overestimation, we adjusted precipitation at elevations >3900 m AMSL by comparing water-balance calculations of surface runoff with hydrometric data (2000–2001) at the Yingluoxia station (Zhangye sub-basin; Fig. 1). This correction was applied uniformly, irrespective of location and time period.

The snowmelt model (Matin and Bourque, 2013b) uses temperature-based separation thresholds for the two precipitation phases (rain and snow). Critical temperatures for snow (T_{snow}) and rain (T_{rain}) apportion precipitation into its components for temperatures between these two thresholds (Bourque and Matin, 2012); T_{snow} is set at −1 °C (McCabe and Markstrom, 2007), whereas T_{rain} is set at +2 °C, following Brown et al. (2003). Within these limits (i.e., T_{snow} and T_{rain}), apportionment of precipitation (P, in mm) is based on:

$$P^k_{snow_{i,j}} = \begin{cases} P^k_{i,j}; & \text{if } T^k_{i,j} < T_{snow} \\ P^k_{i,j} \times \left[\dfrac{T_{rain} - T^k_{i,j}}{T_{rain} - T_{snow}}\right]; & \text{if } T_{snow} \le T^k_{i,j} \le T_{rain}, \\ 0; & \text{if } T^k_{i,j} > T_{rain} \end{cases} \quad (5)$$

and

$$P^k_{rain_{i,j}} = P^k_{i,j} - P^k_{snow_{i,j}}, \quad (6)$$

where "i" and "j" refer to a specific pixel (grid cell) row and column number in an image and $T_{i,j}$ is the monthly average near-surface air temperature at a specific pixel-location "i,j".

A melting degree-day method is used to calculate monthly snowmelt; melting degree-day factor is defined as snowmelt rate per day per unit of temperature (i.e., mm d^{-1} °C^{-1}):

$$SMM^k_{i,j} = \begin{cases} 0.0; & \text{if } T^k_{i,j} < 0°C \\ T^k_{i,j} \times D_k \times DDF_{i,j}; & \text{if } T^k_{i,j} \ge 0°C \end{cases}, \quad (7)$$

where $SMM^k_{i,j}$ is the maximum amount of snow melted (mm) at pixel-location i,j during month k, D_k is the number of days in month k, and $DDF_{i,j}$ is the melting degree-day factor defined according to elevation (Ma and Cheng, 2003), i.e., 3.5 mm d^{-1} °C^{-1} for elevations < 3300 m and 2.5 mm d^{-1} °C^{-1} for elevations ≥ 3300 m AMSL. Accumulated snow (in snow water equivalence, SWE; in mm) in the current month (k) is calculated based on the previous month's (k−1) accumulation, i.e.,

$$SWE^k_{i,j} = \begin{cases} 0.0; & \text{if } SWE^{k-1}_{i,j} + P^k_{snow_{i,j}} \le SMM^k_{i,j} \\ SWE^{k-1}_{i,j} + P^k_{snow_{i,j}} - SMM^k_{i,j}; & \text{if } SWE^{k-1}_{i,j} > SMM^k_{i,j} \end{cases}. \quad (8)$$

Monthly snowmelt (mm) is defined as:

$$SM^k_{i,j} = \begin{cases} SWE^k_{i,j}; & \text{if } SMM^k_{i,j} > SWE^k_{i,j} \\ SMM^k_{i,j}; & \text{if } SMM^k_{i,j} \le SWE^k_{i,j} \end{cases}. \quad (9)$$

For additional detail concerning the development of precipitation and snowmelt surfaces for the current work, refer to Matin and Bourque (2013b).

3.3. Evapotranspiration

Calculation of monthly AET (in mm) for the study area is based on an application of the complementary method of Venturini et al. (2008) and MODIS-based input data (Matin and Bourque, 2013a), i.e.,

$$AET = \alpha \frac{EF_r \Delta}{\lambda \cdot (EF_r \Delta + \gamma)} (R_n - G), \quad (10)$$

$$EF_r = \frac{AET}{PET} = \frac{T_u - T_d}{T_s - T_d}, \quad (11)$$

and

$$T_u = \frac{e^s_s - e_a - \Delta_d T_s + \Delta_s T_d}{\Delta_s - \Delta_d}, \quad (12)$$

where R_n−G is the net available energy, R_n and G are net radiation and soil heat flux (in W m^{-2}), α is the Priestley-Taylor constant (i.e., 1.26, non-dimensional), λ is the latent heat of vaporization (i.e., 2.26×10^6 J kg^{-1}), EF_r is the relative evaporation fraction, T_u is the temperature at which a surface becomes saturated without changes in water vapor pressure, T_s is the land surface temperature (°C), e_a and e^s_s (in hPa) are the actual and saturated vapor pressure at T and T_s, and Δ, Δ_s, and Δ_d (hPa °C^{-1}) are the slopes of the water-vapor-pressure vs. temperature curve at T, T_s, and T_d, respectively. Description of various data products employed in the calculation of AET are summarized in Table 1.

3.4. Groundwater recharge and baseflow

The amount of net GW recharge (in mm) is calculated as the difference between saturated water storage capacity and the FC of the soil complex, i.e.,

$$GW_k = \begin{cases} 0.0; & \text{if } WS_{k-1} \le WS_{FC} \\ (WS_{k-1} - WS_{FC}); & \text{if } WS_{k-1} > WS_{FC} \end{cases}. \quad (13)$$

Groundwater recharge (i.e., GW_k) contributes to the GW storage (GWS), part of which adds to river runoff as baseflow during the recession period (i.e., roughly the September-through-March period of each year). In general, the contribution of baseflow is difficult to assess. The amount of baseflow depends on various factors, including porosity of soil layers, horizontal hydraulic conductivity, slope of GW-table to river-water level, height of the GW-table, and so on. During the wet season, when soils are saturated, the contribution of baseflow to surface runoff is minor compared to direct mountain runoff. Baseflow is estimated as a fraction of GWS

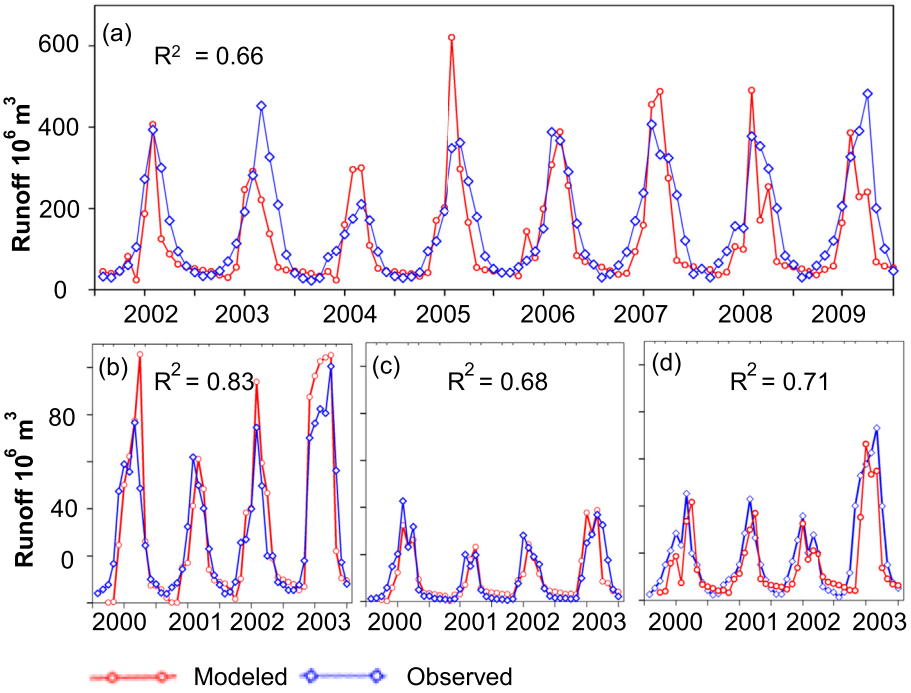

Fig. 5. Comparison of observed (blue line) vs. modeled runoff (red line) at Yingluoxia (a), Xiying (b), Jinta (c), and Zamusi (d) hydrometric stations. (For interpretation of the references to color in this figure legend, the reader is referred to the web version of this article.)

during the recession period, and

$$Q_k^{bf} = C_r \cdot GWS_{k-1}, \quad (14)$$

with

$$GWS_k = GWS_{k-1} + GW_k - Q_k^{bf}, \quad (15)$$

where Q_k^{bf} is the baseflow (in mm) and C_r is a recession parameter (non-dimensional, set during model calibration).

3.5. Runoff-routing

The routing of excess water (Q_k^o) is based on the determination of flow path and volumes from the DEM and slope of source cells to neighboring cells (He et al., 2012). We use the deterministic eight node (D8) algorithm of O'Callaghan and Mark (1984), the most commonly used single-direction routing method. With this

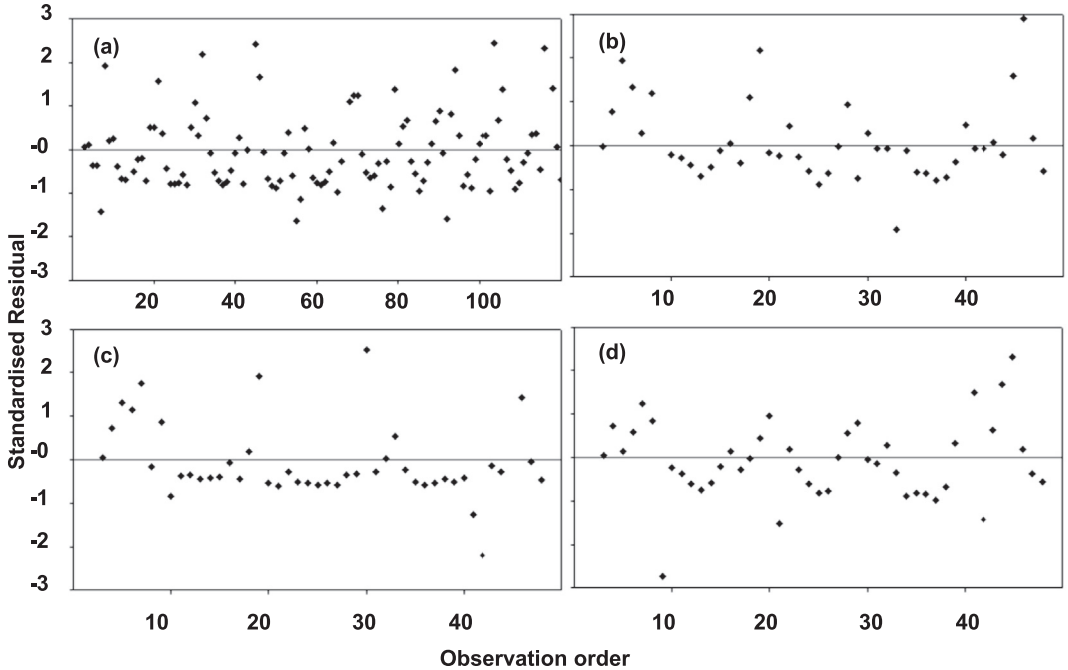

Fig. 6. Residual plots of observations vs. predictions at Yingluoxia (a), Xiying (b), Jinta (c), and Zamusi hydrometric stations (d). Data sources for the observed data for Yingluoxia station come from Yin et al. (2012; their Fig. 4) and for Xiying, Jinta, and Zamusi stations, from Huo et al. (2012; their Fig. 6).

Table 2
Quantitative statistics of model performance in terms of river runoff (including units; lack of units indicates non-dimensional quantities).

	Yingluoxia (2002–2009)	Xiying (2000–2003)	Jinta (2000–2003)	Zamusi (2000–2003)
Slope	0.76	0.72	0.96	0.98
Intercept ($\times 10^6$ m^3)	67.19	7.91	1.22	4.49
r	0.81	0.91	0.85	0.84
R^2	0.66	0.83	0.72	0.71
NSE	0.57	0.79	0.56	0.94
RMSE ($\times 10^6$ m^3)	80.05	12.64	6.26	4.43
RSR	0.66	0.46	0.53	0.25
PBIAS (%)	17.31	−3.88	7.91	21.48

method, flow direction within each cell is calculated as the direction from the center of the source cell to the center of the cell with the lowest elevation among the eight neighboring cells. For routing flow, total outgoing flow is assigned to the cell that is determined by the flow direction. The D8-method is unable to model divergent flows common to flat terrain (Tribe, 1992; Wilson et al., 2007). As the study area is dominated by steep, rugged terrain we do not expect the limitations of the D8-method to be a problem in the current application.

4. Model initialization

Initial values have significant influence on model results. To minimize initialization error, it is assumed that soil water content for any month of the year is not largely different from the average soil water content of the same month over the study years (Xiong and Guo, 1999). The average soil water content is calculated from

$$WS_{0,k} = \frac{\sum_{i=0}^{\eta} WS_{i,k}}{\eta}, \quad (16)$$

where "η" is the number of years (10, in this case).

5. Model calibration

Correction factors for precipitation for mountain elevations >3,900 m AMSL and baseflow recession (i.e., C_r) were calibrated by manually fitting modeled river flow projections to flow data from the Yingluoxia hydrometeric station (Fig. 1) collected over a two-year period (2000–2001). For the current study, we determined the correction factors for precipitation and baseflow recession to be approximately 0.6 and 0.33, respectively.

6. Model validation

The accuracy required from models depend on the objectives for developing the models (Refsgaard and Knudsen, 1996). While various goodness-of-fit statistics have been developed and used to evaluate the quality of hydrological models, ASCE (1993) recommends the use of at least one dimensionless statistic, one absolute error indicator along with some descriptive statistics, and at least one graphical comparison. Moriasi et al. (2007) provided a review of existing quantitative techniques for model validation and classifies them into three main groups: (a) regression statistics, e.g., coefficients of determination (i.e., R^2); (b) dimensionless statistics; and (c) error indices, including the Nash-Sutcliffe modeling efficiency (NSE; Nash and Sutcliffe, 1970), percent bias (PBIAS), percent volume error (D_v), and ratio of root mean squared error (RMSE) to the standard deviation (RSR). We use acceptance thresholds of various evaluation criteria from the literature, i.e., $R^2 > 0.6$, NSE > 0.5, RSR < 0.7, PBIAS within ±25% (Moriasi et al., 2007; Santhi et al., 2001) in assessing model performance. A D_v-value is considered *very good*, when <10%; *good*, when between 10–15%; and *fairly good*, when between 15–25% (Singh et al., 2004).

Validation of model results is conducted by comparing model generated monthly- or annually-accumulated runoff at several hydrometric stations (identified in Fig. 1). In the absence of observations from original sources, we use data from previous studies, including those of Huo et al. (2012), Jia et al. (2010), Wonderen et al. (2010), and Yin et al. (2012). The model was validated against runoff data from one hydrometric station in the Hei River basin (Yingluoxia; Fig. 1) collected over 2002–2009 and three hydrometric stations in the Shiyang River basin (Xiying, Jinta, and Zamusi) collected over 2000–2003. As most of the water to the oases is generated in the mountains, the model was validated for upstream locations of the oases. Deviation from model calculations in the downstream locations (downstream of the oases) is largely expected to be associated with the withdrawal of river water in cropland irrigation.

7. Results and discussion

7.1. Model performance

Monthly modeled and observed hydrographs at the four "validation" stations are presented in Fig. 5. Annual and seasonal patterns in the observed data are captured fairly well when compared against predicted river flow (mountain runoff) determined at the hydrometric stations (Fig. 1). Graphical comparisons do not reveal any systematic bias in model results; observed discrepancy is largely balanced, as illustrated in the residual plots (Fig. 6). The peak flow is also captured fairly well across most years. Quantitative estimates of model performance are presented in Table 2. Statistical assessments of R^2, NSE, and RSR at the Yingluoxia hydrometric station (Fig. 1) are 0.66, 0.57, and 0.66, respectively, suggesting that model predictions are within acceptable limits for the Hei River basin (Moriassi et al., 2007; Santhi et al., 2001). When observed data are presented as functions of predicted data at the Yingluoxia station, the slope and intercept of the fitted regression

Table 3
Annual volume error (% of observed data) between observed and modeled runoff.

Year	Yingluoxia	Xiying	Jinta	Zamusi
2000	15[a]	−2	21	20
2001	25[a]	15	−3	15
2002	25	−18	4	12
2003	33	−8	1	28
2004	−7	–	–	–
2005	2	–	–	–
2006	6	–	–	–
2007	12	–	–	–
2008	23	–	–	–
2009	31	–	–	–
Overall	**17**	**−4**	**7**	**21**

[a] These values were derived from the calibration data and are not included in the computation of overall annual volume error associated with model validation.

line to the comparison data-pairs are 0.76 and 67.19 × 10^6 m^3. These values and a PBIAS of +17.3% indicate that the model, on average, slightly underpredicts actual runoff. Overall absolute error in volume at the Yingluoxia station is 17% yr^{-1}. Year-to-year comparisons (Table 3) show that the absolute error in volume is <10% (very good) for three years, between 10 and 25% (good to fairly good) for three years, and >25% (less than good) for two years.

Coefficient of determination (R^2), NSE, and RSR at Xiying, Jinta, and Zamusi stations (Shiyang River basin; Fig. 1) are 0.83, 0.79, and 0.46, 0.71, 0.94, and 0.25, and 0.72, 0.56, and 0.53, respectively. These values indicate that the model does a significantly better job predicting runoff in the Shiyang River than in the Hei River network. This discrepancy is mostly attributed to two facts. Firstly, seasonal contribution of glacial meltwater is much less in the Shiyang River system due to smaller glaciated areas in the mountainous-portion of the basin compared to the Hei River basin. Secondly, correction to the total modeled precipitation in the upper Shiyang River basin (Section 3.2) is effectively smaller than the level imposed in the upper Hei River basin, as a result of the smaller effective ground-surface area at elevations > 3900 m AMSL, i.e., 1012 vs. 4435 km^2 for the Shiyang and Hei River basins, respectively. Absolute annual volume errors in the Shiyang River basin fall within acceptable limits for most years considered (Table 3).

The amount of deep percolation to the groundwater aquifer under present conditions constitutes a very small proportion (about 1–2%) of the total surface water passing through the river basin. This is confirmed by chloride mass-balance and isotopic studies of surface and groundwater characteristics of nearby areas (Gates et al., 2008; Ma et al., 2008). Conceivably, accurate input [i.e., in the form of calibrated surfaces (grids) of AET, precipitation, and snowmelt; Matin and Bourque, 2013a, 2013b] into a simple water-balance model, as developed in this study, can lead to reasonable estimates of monthly runoff.

7.2. Water yield and soil moisture

Monthly water yield is calculated as the balance of precipitation, snowmelt, and AET. Spatially-distributed mean monthly water yields, based on ten years of data, are shown in Fig. 7. In general, the water balance is negative in the lowlands and oasis-region for most of the year. These illustrations support the notion that AET in the lowlands is generally greater than the water generated from precipitation and snowmelt produced locally, contributing to the

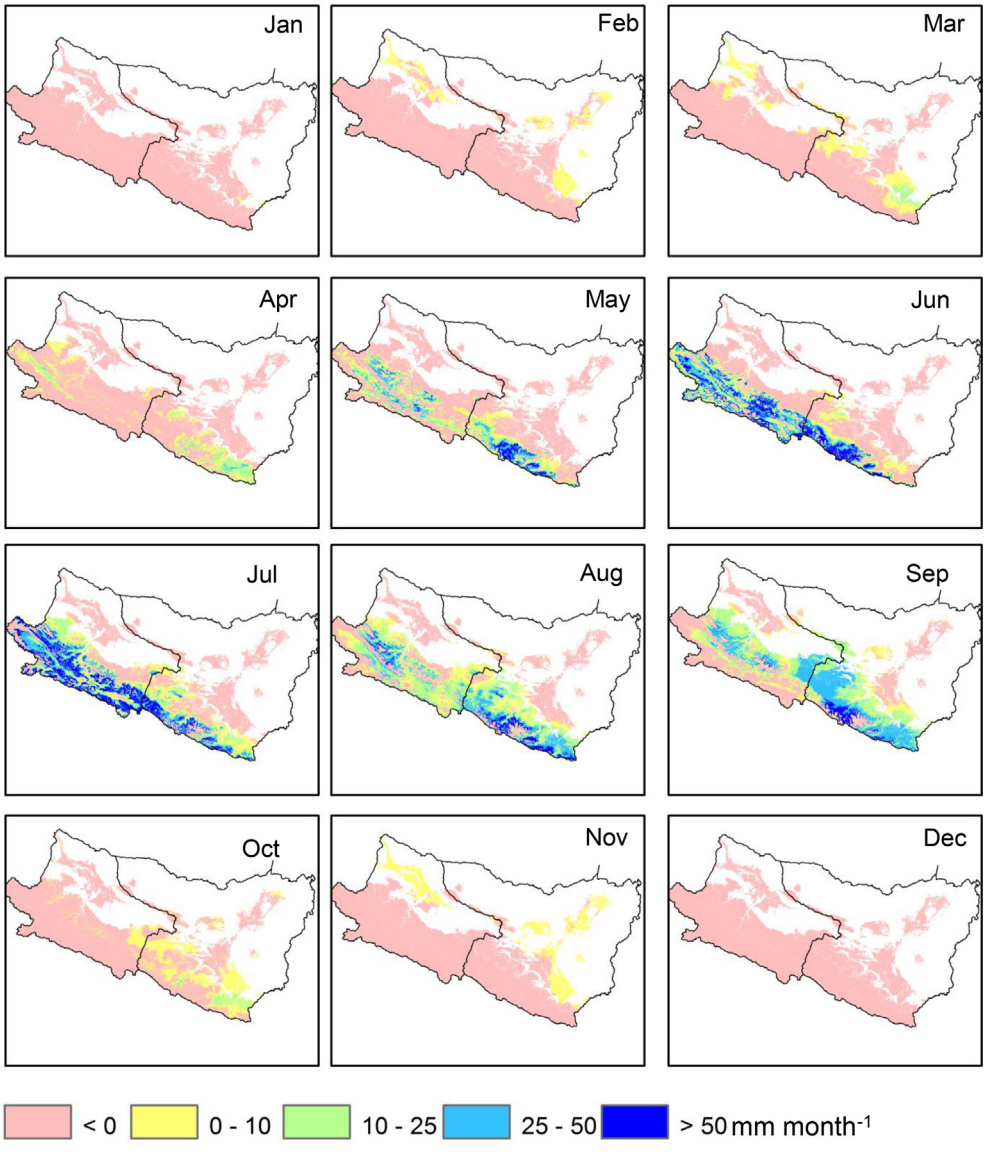

Fig. 7. Average monthly water yield. Monthly averages were calculated from 10-years of modeled results (2000–2009).

aridity of the area. The only source of water to the oases and lower region of the mountains are from mountain surpluses. Precipitation and snowmelt totals surpass AET in mountainous regions during April in the Shiyang and May in the Hei River basins. Ten-year averages of monthly soil moisture (Fig. 8) shows that soils in the oases remain mostly dry (soil water content <15% of soil water capacity) throughout the year. This suggests that agricultural activities in this region largely depend on surface water generated in the mountains. The cropping season in the region is from April–September (Fan et al., 2013; Zhao et al., 2010), which coincides very well with the in-mountain production of liquid water by snowmelt and direct rainfall.

7.3. River-water extraction

To assess the extent of river-water extraction for local usage, modeled results were compared with observed runoff at two downstream locations, i.e., Zhengyxia and Caiqi, downstream of the Zhangye Oasis (Hei River basin) and Liangzhou Oasis (Shiyang River basin; Fig. 1), respectively. River runoff at these locations is largely reduced by the extraction of river water in the support of irrigation in the oases. The comparisons show that the observed runoff is significantly lower than modeled runoff (Fig. 9 a,b). Mean runoff observed at Zhengyxia is about 55% of the runoff projected by the model. Meanwhile, at the Caiqi station, mean observed runoff is about 15% of that modeled, indicating that most of the water flowing from the Qilian Mountains (about 85%) is used in the irrigation of cropland prior reaching the Hongyashan reservoir on the Shiyang River (downstream of Caiqi and at the intersection of the Liangzhou and Minqin Oases; Fig. 1), leaving insufficient water for irrigation in the Minqin Oasis (Fig. 1) and consigning the practice of irrigation in the area to the extraction of brackish groundwater (Aarnoudse et al., 2012; Zong et al., 2011). Over the past 50 years, Minqin Oasis and the lake-district north of the oasis have undergone excessive drying and desertification due to the inordinate amount of river-water extraction upstream (Ma et al., 2007).

8. Contribution of rain and snow to runoff

Mean monthly contribution of rainwater and snowmelt to runoff (Fig. 9c,d) shows that during the March-through-April

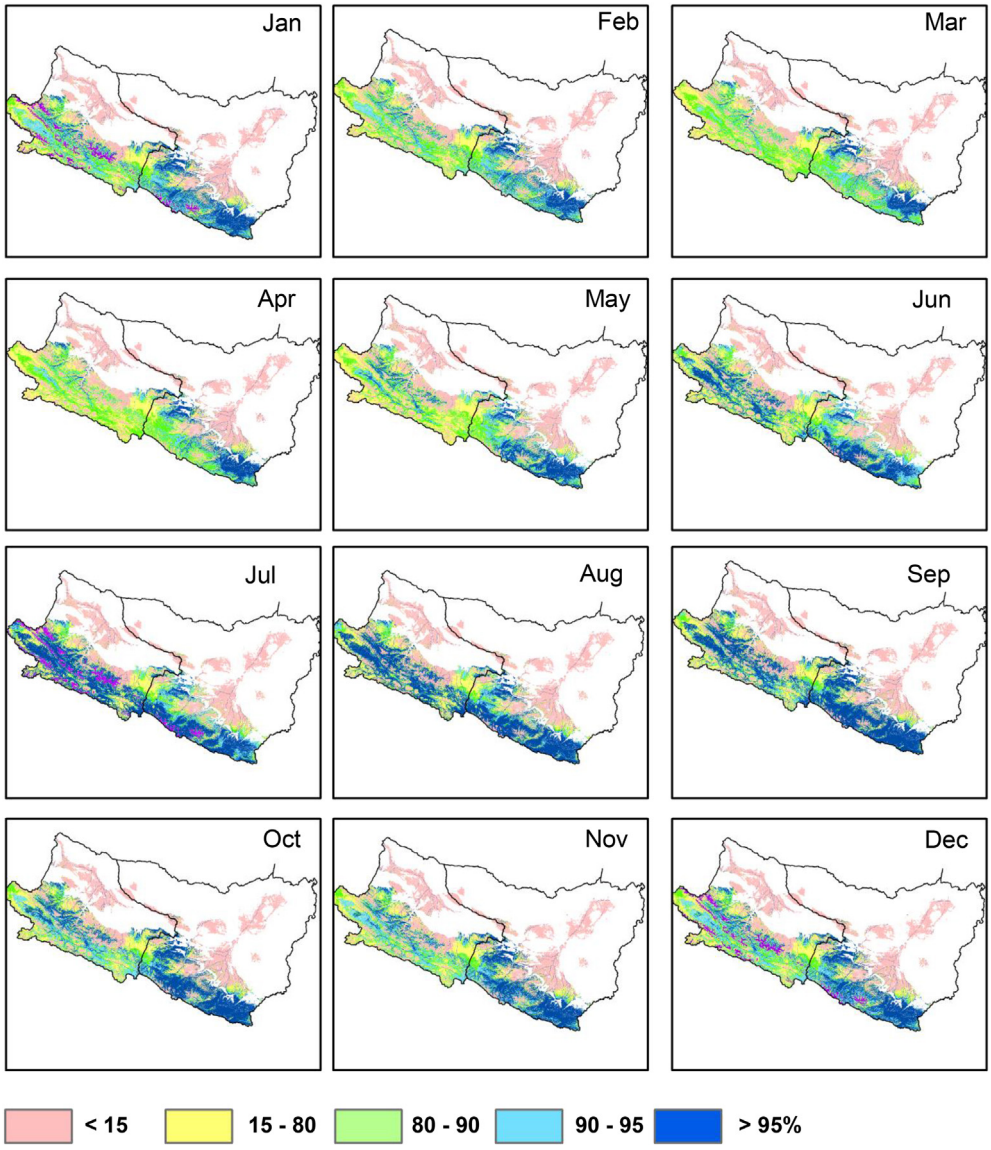

Fig. 8. Average monthly soil moisture for the study area. Monthly averages were calculated from 10-years of modeled results (2000–2009).

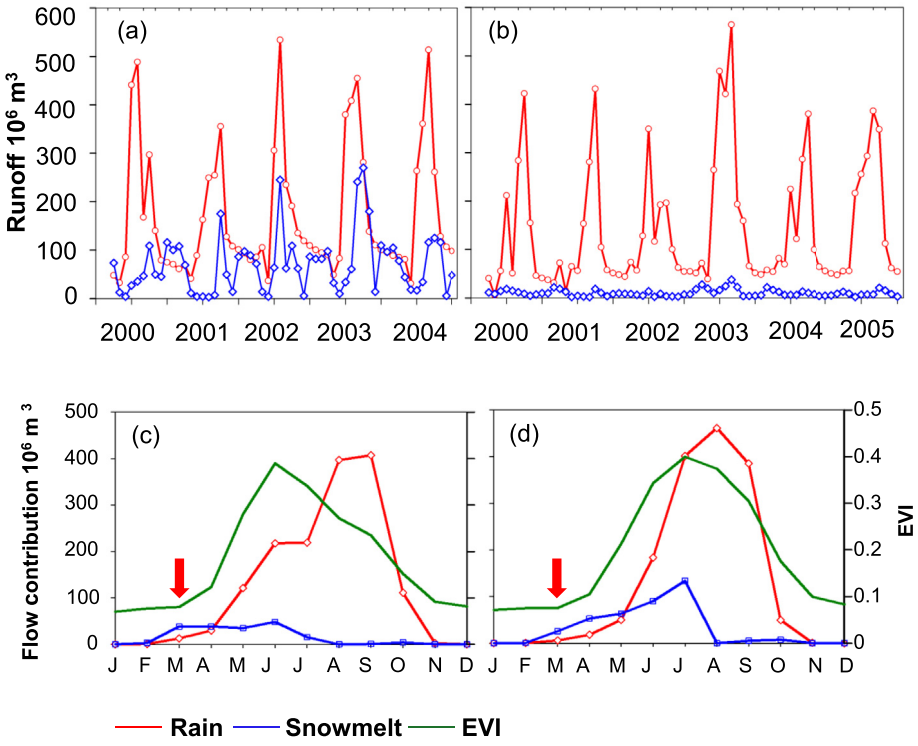

Fig. 9. Comparison of observed (blue line) vs. modeled runoff (red line) at two hydrometric stations downstream of two large oases, i.e., Zhengyxia, downstream of the Zhangye Oasis (a), and Caiqi, downstream of the Liangzhou Oasis (b; Fig. 1) and mean monthly contribution of rainfall (red line) and snowmelt (blue line) to the monthly runoff from the Qilian Mountains and corresponding monthly EVI for the Shiyang River (c) and Hei River basins (d) for the 2000–2009 period. Data sources for the observed data for Zhengyxia come from Jia et al. (2010; their Fig. 6), and for Caiqi station, from Wonderen et al. (2010; their Fig. 5). The red arrow in (c) and (d) indicates the approximate start of the growing season. (For interpretation of the references to color in this figure legend, the reader is referred to the web version of this article.)

period, return flow from the mountains is mostly dominated by snowmelt. This early infusion of water is seen to trigger the greening of the oases in both river basins, as revealed by the sudden increase in enhanced vegetation index in March. Oases development throughtout the growing season is hypothesized to facilitate production of orographic precipitation by increasing the lowland production of water vapor by enhancing AET and subsequent mass transport by wind (Bourque and Matin, 2012). Contribution of orographic rainwater to runoff becomes greatest in August, one to two months after biomass production in the oases reaches its maximum (EVI > 3.5).

9. Conclusions and recommendations

This paper highlights the development of a distributed-hydrological model using RS-based precipitation and modeled AET and snowmelt surfaces (also from RS-data) from previous studies as principal inputs. With slight underprediction, the model produced satisfactory results in comparison with observed runoff data from both the Shiyang and Hei River basins. Because the model does not account for glacial meltwater (which varies from year to year) in the water-balance calculations of individual river basins, the model slightly underpredicted annual water yields for locations in the upper reaches of the Hei River system. Better agreement was obtained for the upper Shiyang River system, as within-basin mountains support fewer large glaciers. Greatest disagreement between observed and modeled runoff was observed for hydrometric stations downstream of major oases, where river water is routinely diverted for irrigation. The study demonstrates the importance of early snowmelt in triggering vegetation growth in oases at the base of the Qilian Mountains. This growth, and subsequent growth to ensue, is hypothesized to contribute to the progressive increase in precipitation production in the mountains, resulting in increased return flow to the oases in the latter part of the summer.

The paper demonstrates the importance RS-data and distributed modeling can have in assessing the hydrological cycle and its components in poorly-monitored arid to semi-arid river basins. While the model captures surface water runoff and associated yields with some level of accuracy, minor discrepancies between actual and modeled yields remain. Future studies are recommended to investigate the contribution of glacial meltwater to the overall runoff from the mountains. Statistics on river-water extraction for irrigation would also be helpful in confirming downstream river yields estimated in this study.

Acknowledgment

This study was jointly funded by: (i) the Lanzhou Regional Climate Centre of the Gansu Provincial Meteorological Bureau (GMB), Lanzhou, China (Natural Science Foundation of China, Grant Number 40830957), and (ii) the Faculty of Forestry and Environmental Management, University of New Brunswick, New Brunswick, Canada. We would like to acknowledge the US *National Aeronautics and Space Administration* (NASA) and *Geological Survey* (USGS) for providing MODIS and SRTM v. 4 DEM data free of charge. We would also like to acknowledge two anonymous reviewers for their helpful suggestions with improving the manuscript.

References

Aarnoudse, E., Bluemling, B., Wester, P., Qu, W., 2012. The role of collective

groundwater institutions in the implementation of direct groundwater regulation measures in Minqin County, China. Hydrogeol. J. 20 (7), 1213–1221. http://dx.doi.org/10.1007/s10040-012-0873-z.
Aghakouchak, A., Habib, E., 2010. Application of a conceptual hydrologic model in teaching hydrologic processes. Int. J. Eng. Edu. 26, 963–973.
Akiyama, T., Sakai, A., Yamazaki, Y., Wang, G., Fujita, K., Nakawo, M., Kubota, J., Konagaya, y, 2007. Surfacewater-groundwater interaction in the Heihe River Basin, Northwest China. Bull. Glaciol. Res. 24, 87–94.
Arnold, J.G., Moriasi, D.N., Gassman, P.W., Abbaspour, K.C., White, M.J., Srinivasan, R., Santhi, C., Harmel, R.D., van Griensven, A., van Liew, M.W., Kannan, N., Jha, M.K., 2012. SWAT: model use, calibration, and validation. Trans. ASABE 55 (4), 1491–1508.
ASCE, 1993. Criteria for evaluation of watershed models. J. Irrig. Drain. Eng.-ASCE 119 (3), 429–442.
Bagchi, A.K., 1982. Orographic variation of precipitation in a high-rise Himalayan Basin. Hydrological aspects of alpine and high-mountain areas. Hydrol. Sci. J.-J. Des. Sci. Hydrol. 27 (2), 250–250.
Beven, K.J., Kirkby, M.J., 1979. A physically based, variable contributing area model of basin hydrology (Un modèle à base physique de zone d'appel variable de l'hydrologie du bassin versant). Hydrol. Sci. Bull. 24 (1), 43–69. http://dx.doi.org/10.1080/02626667909491834.
Bourque, C.P.-A., Hassan, Q.K., 2009. Vegetation control in the long-term self-stabilization of the Liangzhou Oasis of the upper Shiyang River watershed of westcentral Gansu, Northwest China. Earth Interact. 13, 1–22. http://dx.doi.org/10.1175/2009ei286.1.
Bourque, C.P.-A., Matin, M.A., 2012. Seasonal snow cover in the Qilian Mountains of Northwest China: Its dependence on oasis seasonal evolution and lowland production of water vapour. J. Hydrol. 454, 141–151. http://dx.doi.org/10.1016/j.jhydrol.2012.06.008.
Brown, R.D., Brasnett, B., Robinson, D., 2003. Gridded North American monthly snow depth and snow water equivalent for GCM evaluation. Atmos.-Ocean 41 (1), 1–14. http://dx.doi.org/10.3137/Ao.410101.
Carpenter, C., 2001a. Alashan Plateau Semi-desert (PA1302). https://secure.worldwildlife.org/wildworld/profiles/terrestrial/pa/pa1302_full.html (accessed 13.12.12.).
Carpenter, C., 2001b. Montane Grasslands and Shrublands. http://www.worldwildlife.org/science/wildfinder/profiles/pa1015.html (accessed 13.12.12.).
CGIAR-CSI, 2008. SRTM 90-m Digital Elevation Data. http://srtm.csi.cgiar.org/ (accessed 16.12.11.).
Chen, R., Kang, E., Yang, J., Zhang, J., 2003. A distributed runoff model for inland mountainous river basin of Northwest China. J. Geogr. Sci. 13 (3), 363–372.
Chen, Y., Zhang, D.Q., Sun, Y.B., Liu, X.N., Wang, N.Z., Savenije, H.H.G., 2005. Water demand management: a case study of the Heihe River Basin in China. Phys. Chem. Earth 30 (6–7), 408–419. http://dx.doi.org/10.1016/j.pce.2005.06.019.
Chu, P.C., Lu, S.H., Chen, Y.C., 2005. A numerical modeling study on desert oasis self-supporting mechanisms. J. Hydrol. 312 (1–4), 256–276. http://dx.doi.org/10.1016/j.jhydrol.2005.02.043.
Davidson, A., Wang, S.S., 2005. Spatiotemporal variations in land surface albedo across Canada from MODIS observations. Can. J. Remote Sens. 31 (5), 377–390.
Elshorbagy, A., Corzo, G., Srinivasulu, S., Solomatine, D.P., 2009. Experimental investigation of the predictive capabilities of data driven modeling techniques in hydrology – Part 2: application. Hydrol. Earth Syst. Sci. Discuss. 6 (6), 7095–7142. http://dx.doi.org/10.5194/hessd-6-7095-2009.
Elshorbagy, A., Corzo, G., Srinivasulu, S., Solomatine, D.P., 2010. Experimental investigation of the predictive capabilities of data driven modeling techniques in hydrology – Part 1: concepts and methodology. Hydrol. Earth Syst. Sci. 14 (10), 1931–1941. http://dx.doi.org/10.5194/hess-14-1931-2010.
Fan, Z.L., Chai, Q., Huang, G.B., Yu, A.Z., Huang, P., Yang, C.H., Tao, Z.Q., Liu, H.L., 2013. Yield and water consumption characteristics of wheat/maize intercropping with reduced tillage in an Oasis region. Eur. J. Agron. 45, 52–58. http://dx.doi.org/10.1016/j.eja.2012.10.010.
Forth, H.D., 1990. Fundamental of Soil Science. John Wiley and Sons, New York.
Gao, B.C., Kaufman, Y.J., 2003. Water vapor retrievals using moderate resolution imaging spectroradiometer (MODIS) near-infrared channels. J. Geophys. Res.-Atmos. 108 (D13). D13, ACH (4-1) – ACH (4-10). http://dx.doi.org/10.1029/2002jd003023.
Gao, Y., Wang, G., Liu, H., Liu, Z., Lin, W., Wang, J., 2006. Landform Effects the Distribution and Circular Mode on Groundwater in Shiyang River Basin. Beiging, China. http://en.cgs.gov.cn/Achievement/The34thCongress/Evolutional/18050.htm (accessed 03.07.13.).
Gates, J.B., Edmunds, W.M., Darling, W.G., Ma, J.Z., Pang, Z.H., Young, A.A., 2008. Conceptual model of recharge to southeastern Badain Jaran Desert groundwater and lakes from environmental tracers. Appl. Geochem. 23 (12), 3519–3534. http://dx.doi.org/10.1016/j.apgeochem.2008.07.019.
Gu, J., Li, X., Huang, C.L., 2008. Land cover classification in Heihe River Basin with time series MODIS NDVI data. In: Fifth International Conference on Fuzzy Systems and Knowledge Discovery, vol. 2, Proceedings, pp. 477–481. http://dx.doi.org/10.1109/Fskd.2008.517.
Han, D., Meng, X.Y., 1999. Recent progress of research on oasis in China. Chin. Geogr. Sci. 3, 199–205.
He, X., Huang, N., Huang, D., 2012. Research and application on digital river network extraction modified routing algorithm based on DEM. In: Systems and Informatics (ICSAI), 2012 International Conference on, pp. 1728–1731.
Huang, J., van den Dool, H.M., Georgarakos, K.P., 1996. Analysis of model-calculated soil moisture over the United States (1931–1993) and applications to long-range temperature forecasts. J. Clim. 9 (6), 1350–1362 http://dx.doi.org/10.1175/1520-0442(1996)009<1350:aomcsm>2.0.co;2.
Huete, A.R., Didan, K., Miura, T., Rodriguez, E.P., Gao, X., Fereira, L.G., 2002. Overview of the radiometric and biophysical performance of the MODIS vegetation indices. Remote Sens. Environ. 83 (1–2), 195–213. http://dx.doi.org/10.1016/S0034-4257(02)00096-2.
Huete, A.R., Litu, H.Q., Batchily, K., Leeuwen, W.V., 1997. A comparison of vegetation indices over a global set of TM images for EOS-MODIS. Remote Sens. Environ. 59 (3), 440–451. http://dx.doi.org/10.1016/S0034-4257(96)00112-5.
Huo, Z.L., Feng, S.Y., Kang, S.Z., Dai, X.Q., Li, W.C., Chen, S.J., 2007. The response of water-land environment to human activities in arid Minqin oasis, northwest China. Arid Land Res. Manag. 21 (1), 21–36. http://dx.doi.org/10.1080/15324980601087448.
Huo, Z.L., Feng, S.Y., Kang, S.Z., Huang, G.H., Wang, F.X., Guo, P., 2012. Integrated neural networks for monthly river flow estimation in arid inland basin of Northwest China. J. Hydrol. 420, 159–170. http://dx.doi.org/10.1016/j.jhydrol.2011.11.054.
Huo, Z.L., Feng, S.Y., Kang, S.Z., Li, W.C., Chen, S.J., 2008. Effect of climate changes and water-related human activities on annual stream flows of the Shiyang river basin in and North-West China. Hydrol. Process. 22 (16), 3155–3167. http://dx.doi.org/10.1002/Hyp.6900.
Immerzeel, W.W., Gaur, A., Zwart, S.J., 2008. Integrating remote sensing and a process-based hydrological model to evaluate water use and productivity in a south Indian catchment. Agric. Water Manag. 95 (1), 11–24. http://dx.doi.org/10.1016/j.agwat.2007.08.006.
Ji, X.B., Kang, E.S., Chen, R.S., Zhao, W.Z., Zhang, Z.H., Jin, B.W., 2006. The impact of the development of water resources on environment in arid inland river basins of Hexi region, Northwestern China. Environ. Geol. 50 (6), 793–801. http://dx.doi.org/10.1007/s00254-006-0251-z.
Jia, L., Shang, H., Menenti, M., 2010. Vegetation response to upstream water yield in the Heihe river by time series analysis of MODIS data. Hydrol. Earth Syst. Sci. Discuss. 7 (4), 4177–4218. http://dx.doi.org/10.5194/hessd-7-4177-2010.
Jia, Y., Ding, X., Qin, C., Wang, H., 2009. Distributed modeling of landsurface water and energy budgets in the inland Heihe river basin of China. Hydrol. Earth Syst. Sci. 13 (10), 1849–1866.
Jin, X.M., Schaepman, M., Clevers, J., Su, Z.B., Hu, G.C., 2010. Correlation between annual runoff in the Heihe River to the vegetation cover in the Ejina Oasis (China). Arid Land Res. Manag. 24 (1), 31–41. http://dx.doi.org/10.1080/15324980903439297.
Kang, E.S., Cheng, G.D., Lan, Y.C., Jin, H.J., 1999. A model for simulating the response of runoff from the mountainous watersheds of inland river basins in the arid area of northwest China to climatic changes. Sci. China Ser. D-Earth Sci. 42, 52–63. http://dx.doi.org/10.1007/Bf02878853.
Kang, S.Z., Su, X.L., Tong, L., Shi, P.Z., Yang, X.Y., Abe, Y.K., Du, T.S., Shen, Q.L., Zhang, J.H., 2009. The impacts of human activities on the water-land environment of the Shiyang River basin, an arid region in northwest China. Hydrol. Sci. J.-J. Des. Sci. Hydrol. 49 (3), 413–427. http://dx.doi.org/10.1623/hysj.49.3.413.54347.
Kaufman, Y.J., Gao, B.C., 1992. Remote sensing of water vapor in the near IR from EOS/MODIS. IEEE Trans. Geosci. Remote Sens. 30 (5), 871–884. http://dx.doi.org/10.1109/36.175321.
Kishtawal, C.M., Basu, S., Patadia, F., Thapliyal, P.K., 2003. Forecasting summer rainfall over India using genetic algorithm. Geophys. Res. Lett. 30, 23. http://dx.doi.org/10.1029/2003gl018504.
Kite, G.W., Pietroniro, A., 1996. Remote sensing applications in hydrological modelling. Hydrol. Sci. J.-J. Des. Sci. Hydrol. 41 (4), 563–591. http://dx.doi.org/10.1080/02626669609491526.
Kobayashi, T., Matsuda, S., Nagai, H., Tesima, J., 2001. A bucket with a bottom hole (BBH) model of soil hydrology. Soil-Veg.-Atmos. Transf. Schemes Large-Scale Hydrol. Models 270, 41–45.
Li, F., Zhu, G., Guo, C., 2013. Shiyang River ecosystem problems and countermeasures. Agric. Sci. 4 (2), 72–78. http://dx.doi.org/10.4236/as.2013.42012.
Li, X.Y., Xiao, D.N., He, X.Y., Chen, W., Song, D.M., 2006. Dynamics of typical agricultural landscape and its relationship with water resource in inland Shiyang River watershed, Gansu Province, northwest China. Environ. Monit. Assess. 123 (1–3), 199–217. http://dx.doi.org/10.1007/s10661-006-9191-z.
Li, X.Y., Xiao, D.N., He, X.Y., Chen, W., Song, D.M., 2007. Factors associated with farmland area changes in arid regions: a case study of the Shiyang River Basin, Northwestern China. Front. Ecol. Environ. 5 (3), 139–144. http://dx.doi.org/10.1890/1540-9295(2007)5[139:Fawfac]2.0.Co;2.
Li, Z.L., Xu, Z.X., Li, J.Y., Li, Z.J., 2008. Shift trend and step changes for runoff time series in the Shiyang River Basin, Northwest China. Hydrol. Process. 22 (23), 4639–4646. http://dx.doi.org/10.1002/Hyp.7127.
Liang, X., Wood, E.F., Lettenmaier, D.P., 1996. Surface soil moisture parameterization of the VIC-2L model: evaluation and modification. Glob. Planet. Change 13 (1–4), 195–206. http://dx.doi.org/10.1016/0921-8181(95)00046-1.
Lindstrom, G., Johansson, B., Persson, M., Gardelin, M., Bergstrom, S., 1997. Development and test of the distributed HBV-96 hydrological model. J. Hydrol. 201 (1–4), 272–288. http://dx.doi.org/10.1016/S0022-1694(97)00041-3.
Liu, T., Willems, P., Feng, X.W., Li, Q., Huang, Y., Bao, A.M., Chen, X., Veroustraete, F., Dong, Q.H., 2012. On the usefulness of remote sensing input data for spatially distributed hydrological modelling: case of the Tarim River basin in China. Hydrol. Process. 26 (3), 335–344. http://dx.doi.org/Doi 10.1002/Hyp.8129.
Ma, H., Cheng, G.D., 2003. A test of snowmelt runoff model (SRM) for the Gongnaisi River Basin in the western Tianshan Mountains, China. Chin. Sci. Bull. 48 (20),

2253–2259. http://dx.doi.org/10.1360/03wd0135.
Ma, J.Z., Ding, Z., Gates, J.B., Su, Y., 2008. Chloride and the environmental isotopes as the indicators of the groundwater recharge in the Gobi Desert, northwest China. Environ. Geol. 55 (7), 1407–1419.
Ma, J.Z., Chen, L.H., He, J.H., Zhang, Y.R., Li, X.H., Edmunds, W.M., 2013. Trends and periodicities in observed temperature, precipitation and runoff in a desert catchment: case study for the Shiyang River Basin in Northwestern China. Water Environ. J. 27 (1), 86–98. http://dx.doi.org/10.1111/j.1747-6593.2012.00329.x.
Ma, M.G., Veroustraete, F., 2006. Interannual variability of vegetation cover in the Chinese Heihe River Basin and its relation to meterological parameters. Int. J. Remote Sens. 27 (22), 5127–5127. http://dx.doi.org/10.1080/01431160601103475.
Ma, Y.H., Fan, S.Y., Zhou, L.H., Dong, Z.H., Zhang, K.C., Feng, J.M., 2007. The temporal change of driving factors during the course of land desertification in arid region of North China: the case of Minqin County. Environ. Geol. 51 (6), 999–1008. http://dx.doi.org/10.1007/s00254-006-0369-z.
Manabe, S., 1969. Climate and the ocean circulation: 1. The atmospheric circulation and the hydrology of the earth's surface. Mon. Weather Rev. 97 (11), 739–774.
Matin, M.A., Bourque, C.P.A., 2013b. Intra- and inter-annual variations in snow-water storage in data sparse desert-mountain regions assessed from remote sensing. Remote Sens. Environ. 139, 18–34. http://dx.doi.org/10.1016/j.rse.2013.07.033.
Matin, M.A., Bourque, C.P.A., 2013a. Assessing spatiotemporal variation in actual evapotranspiration for semi-arid watersheds in northwest China: evaluation of two complementary-based methods. J. Hydrol. 486, 455–465. http://dx.doi.org/10.1016/j.jhydrol.2013.02.014.
McCabe, G.J., Markstrom, S.L., 2007. A Monthly Water-balance Model Driven by Graphical User Interface. US Geological Survey-open file report 2007-1088. http://pubs.usgs.gov/of/2007/1088/pdf/of07-1088_508.pdf (accessed 09.06.13.).
Meybeck, M., 2003. Global analysis of river systems: from Earth system controls to anthropocene syndromes. Philos. Trans. R. Soc. B-Biol. Sci. 358 (1440), 1935–1955. http://dx.doi.org/10.1098/rstb.2003.1379.
Miller, A.A., 1961. Climatology. Methuen, London.
Monteith, J.L., 1965. Evaporation and environment. Symp. Soc. Exp. Biol. 19, 205–234.
Moriasi, D.N., Arnold, J.G., Van Liew, M.W., Bingner, R.L., Harmel, R.D., Veith, T.L., 2007. Model evaluation guidelines for systematic quantification of accuracy in watershed simulations. Trans. ASABE 50 (3), 885–900.
Nachtergaele, F., Velthuizen, H.v., Verelst, L., Wberg, D., Batjes, N., Dijkshoorm, K., Engelen, V.v., Fischer, G., Jones, A., Montanarella, L., Petri, M., Prieler, S., Teixeira, E., Shi, X., 2012. Harmonized World Soil Database (Version 1.2). Food and Agriculture Organization of the United Nations (FAO), International Institute for Applied Systems Analysis (IIASA), ISRIC – World Soil Information, Institute of Soil Science – Chinese Academy of Sciences (IISCAS), Joint Research Centre of the European Commission (JRC), Laxenburg, Austria.
Nash, J.E., Sutcliffe, J.V., 1970. River flow forecasting through conceptual models part I – a discussion of principles. J. Hydrol. 10 (3), 282–290. http://dx.doi.org/10.1016/0022-1694(70)90255-6.
Nijssen, B., Lettenmaier, D.P., Liang, X., Wetzel, S.W., Wood, E.F., 1997. Streamflow simulation for continental-scale river basins. Water Resour. Res. 33 (4), 711–724. http://dx.doi.org/10.1029/96wr03517.
O'Callaghan, J.F., Mark, D.M., 1984. The extraction of drainage networks from digital elevation data. Comput. Vision, Graph. Image Process. 28, 328–344.
Olson, D.M., Dinerstein, E., Wikramanayake, E.D., Burgess, N.D., Powell, G.V.N., Underwood, E.C., D'Amico, J.A., Itoua, I., Strand, H.E., Morrison, J.C., Loucks, C.J., Allnutt, T.F., Ricketts, T.H., Kura, Y., Lamoreux, J.F., Wettengel, W.W., Hedao, P., Kassem, K.R., 2001. Terrestrial ecoregions of the world: a new map of life on Earth. BioScience 51 (11), 933–938. http://dx.doi.org/10.1641/0006-3568(2001)051[0933:teotwa]2.0.co;2.
Pechlivanidis, I.G., Jackson, B.M., Mcintyre, N.R., Wheater, H.S., 2011. Catchment scale hydrological modelling: a review of model types, calibration approaches and uncertainty analysis methods in the context of recent developments in technology and applications. Glob. Nest J. 13 (3), 193–214.
Penman, H.L., 1948. Natural evaporation from open water, bare soil and grass. Proc. R. Soc. Lond. Ser. A, Math. Phys. Sci. 193 (1032), 120–145.
Petitcolin, F., Vermote, E., 2002. Land surface reflectance, emissivity and temperature from MODIS middle and thermal infrared data. Remote Sens. Environ. 83 (1–2), 112–134. http://dx.doi.org/10.1016/S0034-4257(02)00094-9.
Pietroniro, A., Leconte, R., 2005. A review of Canadian remote sensing and hydrology, 1999–2003. Hydrol. Process. 19 (1), 285–301. http://dx.doi.org/Doi 10.1002/Hyp.5771.
Qin, C.B., Jia, Y.W., Su, Z., Zhou, Z.H., Qiu, Y.Q., Suhui, S., 2008. Integrating remote sensing information into a distributed hydrological model for improving water budget predictions in large-scale basins through data assimilation. Sensors 8 (7), 4441–4465. http://dx.doi.org/Doi 10.3390/S8074441.
Rakhecha, P.R., Vijay, P.S., 2009. Applied Hydrometeorology. Springer, p. 356.
Refsgaard, J.C., Knudsen, J., 1996. Operational validation and intercomparison of different types of hydrological models. Water Resour. Res. 32 (7), 2189–2202. http://dx.doi.org/10.1029/96wr00896.
Reuter, H.I., Nelson, A., Jarvis, A., 2007. An evaluation of void-filling interpolation methods for SRTM data. Int. J. Geogr. Inf. Sci. 21 (9), 983–1008.
Roe, G.H., 2005. Orographic precipitation. Annu. Rev. Earth Planet. Sci. 33, 645–671.
Romano, N., Palladino, M., Chirico, G.B., 2011. Parameterization of a bucket model for soil-vegetation-atmosphere modeling under seasonal climatic regimes. Hydrol. Earth Syst. Sci. 15 (12), 3877–3893. http://dx.doi.org/10.5194/hess-15-3877-2011.
Santhi, C., Arnold, J.G., Williams, J.R., Dugas, W.A., Srinivasan, R., Hauck, L.M., 2001. Validation of the SWAT model on a large river basin with point and nonpoint sources. J. Am. Water Resour. Assoc. 37 (5), 1169–1188. http://dx.doi.org/10.1111/j.1752-1688.2001.tb03630.x.
Saxton, K.E., Rawls, W.J., 2006. Soil water characteristic estimates by texture and organic matter for hydrologic solutions. Soil Sci. Soc. Am. J. 70, 1569–1578.
Schmugge, T.J., Kustas, W.P., Ritchie, J.C., Jackson, T.J., Rango, A., 2002. Remote sensing in hydrology. Adv. Water Resour. 25 (8–12), 1367–1385. http://dx.doi.org/10.1016/S0309-1708(02)00065-9.
Schultz, G.A., 1993. Hydrological modeling based on remote-sensing information. Adv. Space Res. 13 (5), 149–166. http://dx.doi.org/10.1016/0273-1177(93)90540-R.
Schultz, G.A., 1996. Remote sensing applications to hydrology: Runoff. Hydrol. Sci. J.-J. Des. Sci. Hydrol. 41 (4), 453–475. http://dx.doi.org/10.1080/02626669609491520.
Seeman, S.W., Borbas, E.E., Li, J., Menzel, W.P., Gumley, L.E., 2006. MODIS Atmospheric Profile Retrieval, Algorithm Theoritical Basis Document. Version 6, Reference Number ATBD-MOD07. Cooperative Institute for Meteorological Satellite Studies, Madison, WI. http://modis.gsfc.nasa.gov/data/atbd/atbd_mod07.pdf (accessed 20.06.13.).
Shelp, M.L., Zhan, G.S., Upton, B., 2011. The applications of satellite based remote sensing techniques in the hydrological assessment of mine water supply and management systems. Mine Water Environ. 30 (4), 242–251. http://dx.doi.org/10.1007/s10230-011-0153-5.
Singh, J., Knapp, H.V., Demissie, M., 2004. Hydrological Modeling of the Iroquois River Watershed Using HSPF and SWAT. ISWS CR 2004–08. Illinois State Water Survey, Champaign, Ill. www.sws.uiuc.edu/pubdoc/CR/ISWSCR2004-08.pdf (accessed 05.06.13.).
Tong, L., Kang, S.Z., Zhang, L., 2007. Temporal and spatial variations of evapotranspiration for spring wheat in the Shiyang River Basin in Northwest China. Agric. Water Manag. 87 (3), 241–250. http://dx.doi.org/10.1016/j.agwat.2006.07.013.
Tribe, A., 1992. Automated recognition of valley lines and drainage networks from grid digital elevation models - a review and a new method. J. Hydrol. 139 (1–4), 263–293. http://dx.doi.org/10.1016/0022-1694(92)90206-B.
Venturini, V., Islam, S., Rodriguez, L., 2008. Estimation of evaporative fraction and evapotranspiration from MODIS products using a complementary based model. Remote Sens. Environ. 112 (1), 132–141. http://dx.doi.org/10.1016/j.rse.2007.04.014.
Wan, Z., Zhang, Y., Zhang, Q., Li, Z.L., 2004. Quality assessment and validation of the MODIS global land surface temperature. Int. J. Remote Sens. 25 (1), 261–274. http://dx.doi.org/10.1080/0143116031000116417.
Wang, C., Zhao, C.Y., 2013. TRMM satellite data in the upper reaches of Heihe multiple spatial and temporal characteristics of precipitation research applications (in Chinese). J. Nat. Resour. 28, 5.
Wang, G.X., Cheng, G.D., 1999. Water resource development and its influence on the environment in arid areas of China - the case of the Hei River basin. J. Arid Environ. 43 (2), 121–131.
Wang, J.S., Feng, J.Y., Yang, L.F., Guo, J.Y., Pu, Z.X., 2009a. Runoff-denoted drought index and its relationship to the yields of spring wheat in the arid area of Hexi Corridor, Northwest China. Agric. Water Manag. 96 (4), 666–676. http://dx.doi.org/10.1016/j.agwat.2008.10.008.
Wang, N.L., He, J.Q., Jiang, X., Song, G.J., Pu, J.C., Wu, X.B., Chen, L., 2009b. Study on the zone of maximum precipitation in the north slopes of the central Qilian Mountains (in Chinese). J. Glaciol. Geocryol. 3.
Wang, N., He, J., Pu, J., Jiang, X., Jing, Z., 2010. Variations in equilibrium line altitude of the QiyiGlacier, Qilian Mountains, over the past 50 years. Chin. Sci. Bull. 55 (33), 3810–3817.
Wang, X., Zhao, C., 2011. Analysis of Temporal Trends in Potential Evapotranspiration over Heihe River Basin. Presented in 2011 International Symposium on Water Resource and Environmental Protection (ISWREP), Xi'an, 20–22 May 2011. http://dx.doi.org/10.1109/iswrep.2011.5893130.
Wilson, J.P., Lam, C.S., Deng, Y.X., 2007. Comparison of the performance of flow-routing algorithms used in GIS-based hydrologic analysis. Hydrol. Process. 21 (8), 1026–1044. http://dx.doi.org/10.1002/Hyp.6277.
Wonderen, J.V., Moore, D., Wardlaw, R., Zhongjing, W., Litang, H., Qingling, S., 2010. Water Resources and Modelling in the Shiyang River Basin. Presented in BHS Third international symposium, Managing consequences of a changing global environment, Newcastle.
Wu, Y., Wen, X., Zhang, Y., 2004. Analysis of the exchange of groundwater and river water by using radon-222 in the middle Heihe basin of northwestern China. Environ. Geol. 45 (5), 647–653. http://dx.doi.org/10.1007/s00254-003-0914-y.
Xing, Z., Bourque, C.P.-A., Meng, F.-R., Cox, R.M., Swift, D.E., Zha, T.-S., Chow, L., 2008. A process-based model designed for filling of large data gaps in tower-based measurements of net ecosystem productivity. Ecol. Model. 213, 165–179. http://dx.doi.org/10.1016/j.ecolmodel.2007.11.018.
Xiong, L.H., Guo, S.L., 1999. A two-parameter monthly water balance model and its application. J. Hydrol. 216 (1–2), 111–123. http://dx.doi.org/10.1016/S0022-1694(98)00297-2.
Yang, Z.N., Yang, Z.H., Wang, Q., 1991. Characteristics of hydrological processes in a small high mountain basin. Snow, Hydrol. For. High Alp. Areas 205, 229–236.
Yin, Z., Xiao, H., Zou, S., Wang, W., Lu, Z., Xu, B., 2012. Analysis on water balance in different land cover types at upper reaches of Heihe River basin in

Northwestern China using SWAT model. In: Geomatics for Integrated Water Resources Management (GIWRM), 2012 International Symposium on, pp. 1–6.
Zang, C.F., Liu, J., van der Velde, M., Kraxner, F., 2012. Assessment of spatial and temporal patterns of green and blue water flows under natural conditions in inland river basins in Northwest China. Hydrol. Earth Syst. Sci. 16 (8), 2859–2870. http://dx.doi.org/10.5194/hess-16-2859-2012.
Zhao, C., Nan, Z., Cheng, G., 2005. Methods for estimating irrigation needs of spring wheat in the middle Heihe Basin. China Agric. Water Manag. 75 (1), 54–70. http://dx.doi.org/10.1016/j.agwat.2004.12.003.
Zhao, D., Zhang, W., 2005. Rainfall-runoff simulation using the VIC-3L model over the Heihe River Mountainous Basin, China. In: IGARSS 2005: IEEE International Geoscience and Remote Sensing Symposium, vols. 1–8, Proceedings, pp. 4391–4394.
Zhao, W.Z., Liu, B., Zhang, Z.H., 2010. Water requirements of maize in the middle Heihe River basin, China. Agric. Water Manag. 97 (2), 215–223. http://dx.doi.org/10.1016/j.agwat.2009.09.011.
Zhu, Y.H., Wu, Y.Q., Drake, S., 2004. A survey: obstacles and strategies for the development of ground-water resources in arid inland river basins of Western China. J. Arid Environ. 59 (2), 351–367. http://dx.doi.org/10.1016/j.jaridenv.2003.12.006.
Zong, L., Tedeschi, A., Xue, X., Wang, T., Menenti, M., Huang, C.H., 2011. Effect of different irrigation water salinities on some yield and quality components of two field-grown Cucurbit species. Turkish J. Agric. For. 35 (3), 297–307. http://dx.doi.org/10.3906/Tar-0908-5.